Al-Rubaye GA, Tsimenidis CC, Johnston M.

LDPC-COFDM for PLC in Non-Gaussian Noise Using LLRs Derived from Effective Noise PDFs.

***IET Communications* 2017,**

https://doi.org/10.1049/iet-com.2017.0265

LDPC-COFDM for PLC in Non-Gaussian Noise Using LLRs Derived from Effective Noise PDFs

Ghanim A. Al-Rubaye, Student Member, IEEE, Charalampos C. Tsimenidis, Senior Member, IEEE, and Martin Johnston, Member, IEEE

Abstract

In this paper, the performance of irregular low-density parity check (LPDC) coded orthogonal frequency division multiplexing (COFDM) utilizing 4096 quadrature amplitude modulation (4096-QAM) is investigated over multipath power-line communication (PLC) channel. The effective complex-valued ratio distributions of the noise samples at the zero-forcing (ZF) equalizer output considering both frequency-selective multipath PLCs, background and impulsive noise are derived, in addition to the condition for optimum detection of 4096-QAM and the bit error rate (BER). Moreover, the performance of the LDPC decoder is improved by computing the log-likelihood ratios (LLRs) required for soft decoding based on the derived PDFs. Numerical results obtained using the newly derived LLRs demonstrate a significant performance improvement compared to the conventional receiver that uses blanking impulsive noise mitigation method and LLRs computed based on the Gaussian distribution. Furthermore, EXtrinsic Information Transfer (EXIT) chart analysis demonstrates that the proposed approach requires fewer iterations for convergence compared to the conventional receiver. Finally, utilizing channel bandwidth of 22.4 MHz, the proposed system offers an improvement of 111 Mbps

over the conventional system to reach a maximum data throughput of 256 Mbps for a signal to noise ratio (SNR) of 39 dB and BER of 10^{-5}.

Index Terms

Power-line communication, background noise, impulsive noise, orthogonal frequency division multiplexing, low density parity check code, EXIT chart, zero forcing equalizer.

I. INTRODUCTION

Power-line communication (PLC) channels enable high-speed data transmission and offer economical communication with cheap installation and reliable connection throughout buildings. Therefore, the demand has increased for their utilization as effective media for indoor networks. However, the characteristics of PLC are not specifically designed for communication at high frequencies like other conventional communication channels such as coaxial cables, fiber-optic cables or twisted pair cables. In addition, the PLC channel is a harsh medium for high-speed data transmission due to a large number of reflection points, high attenuation, frequency selectivity and impulsive noise [1]–[3]. Therefore, all of these factors need to be considered in order to establish reliable communication over this medium.

The noise in PLC channel can be classified into colored background interference noise (BI) and impulsive noise (IN) [4]–[6]. The IN has a high power spectral density (PSD) exceeding the PSD of the BI by 10-15 dB [4], [5]. The experimental results presented in [5], [7], demonstrated that in the frequency band 1-30 MHz the amplitude spectrum of the background interference (BI) noise follows the Nakagami-m distribution, while thermal background noise and impulsive noise can be modelled by using Bernoulli-Gaussian mixture (BGM) model or Middleton class A impulsive noise model. Fertonani and Colavolpe [8] showed that impulse noise samples sometimes occur in bursts, hence presenting a channel with memory, referred to as Markovian-

Gaussian channel. However, in past decade, the majority of previous research works follow the memoryless Bernoulli Gaussian mixture model. In practice, the Markovian-Gaussian model reduces to the former Bernoulli Gaussian mixture model when the transition probabilities depend on the arrival state only. Therefore, in our paper we employed the Nakagami-m background interference noise and Bernoulli Gaussian mixture model to make the results more comparable to the results from previous research [9], [10].

The multipath effects and impulsive noise are the dominant performance degradation factors in PLC. To combat both of them, orthogonal frequency division multiplexing (OFDM) has been adopted for broadband PLC standards such as the Home-Plug AV to provide 197 Mbps for high-speed communication [11], [12]. OFDM is commonly used with a cyclic prefix (CP) to convert the frequency-selective multipath into narrowband frequency-flat channels to eliminate inter-symbol interference (ISI); hence, requiring only a simple single-tap equalizer at the receiver [13]. On the other hand, different non-linearity based impulsive noise mitigation methods with different degrees of complexity are used in the time domain to limit the amplitude of impulsive noise samples before the OFDM demodulator. These include clipping, blanking and hybrid methods combining clipping/blanking [6], [14], [15].

Forward error correction (FEC) code with soft iterative decoders such as low-density parity check (LDPC) codes and turbo codes (TC) have been introduced for PLC channels to improve the bit error rate (BER) performance by utilizing frequency diversity [3], [16]. LDPC codes with iterative soft-decision decoding achieves performance very close to the Shannon limit, lower decoding complexity and it is easy to modify the code rates with better BER performance than turbo codes [17], [18]. Therefore, LDPC codes are adopted in this paper. The iterative decoders of these techniques are highly sensitive to the log-likelihood ratio (LLR) computations. For instance, the BER performance of LDPC-COFDM system utilizing LLRs computed based

solely on the Gaussian noise probability density function (PDF) assumption deteriorates quickly over the multipath PLC channel since the effects of the channel multipath on the noise PDF of LLR computation are ignored. This is true even if the impulsive noise assumption is used. Although the PLC noise PDFs are well-known [7], [19], [20], in this paper we derive the PDF of the noise after the channel equalizer. Thus, we define effective noise as the noise samples after the frequency-domain, single-tap, channel equalizer stage required in OFDM systems. Therefore, we focus on the improving the performance of the LDPC decoder by deriving the effective noise PDFs after ZF equalizer and utilizing the outcome in computing the soft LLRs.

Furthermore, EXIT charts are used to demonstrate the improved convergence of the proposed approach over PLC channels in the presence of both background interference noise and impulsive noise [16], [21]. The major contributions of this paper related to the performance analysis of the irregular LDPC-COFDM system over PLC channels are the following:

- We derive the effective noise PDFs at the zero-forcing (ZF) equalizer output for the individual and combined Nakagami-m type BI and BGM models.
- We derive the maximum likelihood detector, the symbol error rate (SER) and the BER for the derived noise PDFs.
- We improve the performance of the LDPC decoder by utilizing the LLRs computed based on the derived noise PDFs over PLC channels. Hence, improving the data throughput.
- We derive the EXIT chart equations based on the derived combined BI and BGM PDF, and we examine their validity against the conventional EXIT chart analysis based on the Gaussian PDF [21].

The rest of the paper is organized as follows. Section II describes the LDPC-COFDM system over PLC channels. Section III shows the effective noise PDFs derivation at the ZF equalizer output. The maximum likelihood detector, LLRs, SER, and BER are derived in section IV. The

EXIT chart analysis of irregular LDPC codes is presented in Section V. Simulations and results are presented in Section VI, and finally, Section VII concludes the paper.

II. LDPC-COFDM SYSTEM OVER PLC CHANNELS

The block-diagram of the LDPC-COFDM system is shown in Fig. 1.

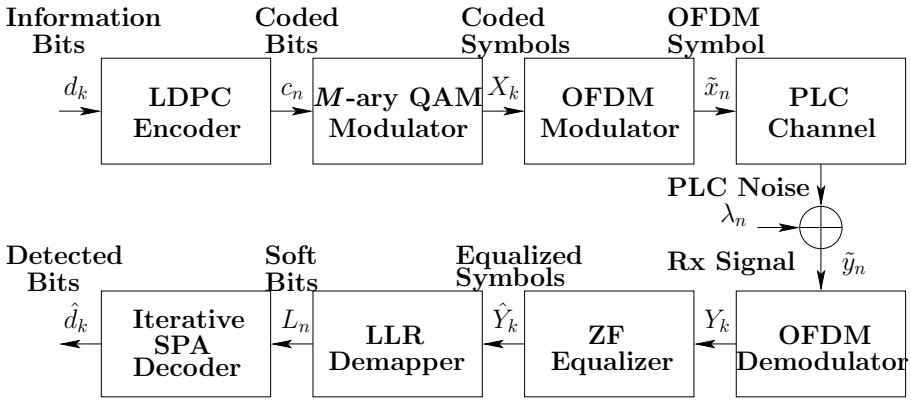

Fig. 1. M-ary QAM LDPC-COFDM system over multipath PLC channel.

LDPC codes belong to a class of FEC, linear block codes originally proposed by Gallager in 1962 [22]. LDPC codes can be classified into regular and irregular codes, in which, the latter type achieve a superior BER performance than the first type. The irregular LDPC codes can be constructed by $(n-k)\times n$ sparse parity check matrix $\mathbf{H}$ with variable column weight, w_c, and the row weight, w_r, respectively [23]. At first, a block of information bits $\mathbf{d}=\{d_0,d_1,\ldots,d_{k-1}\}$ is encoded into codeword $\mathbf{c}=\{c_0,c_1,\ldots,c_{n-1}\}$ using the LDPC encoder. Subsequently, the bits of the codeword $\mathbf{c}$ are first grouped into groups of κ bits and then mapped unto to the 2^κ symbols of a QAM constellation, i.e. for a κ-tuple $\{c_m,c_{m+1},\ldots c_{m+\kappa-1}\}$ of bits the corresponding QAM symbol is $X_k=\mathbf{C}[\sum_{m=0}^{\kappa-1}2^{\kappa-1-m}c_m]$, where $\mathbf{C}\in\mathbb{C}^{2^\kappa\times 1}$ is the Gray-encoded constellation vector.

The complex base-band OFDM signal in the time domain can be implemented using an N-points inverse fast Fourier transform (IFFT) as [24]

$$x_n = \frac{1}{\sqrt{N}} \sum_{k=0}^{N-1} X_k e^{j2\pi kn/N}, n = 0, 1, \cdots, N-1, \tag{1}$$

where N is the number of sub-carriers. To eliminate ISI between consecutive OFDM symbols in PLC channels, a time-domain CP of length N_{CP} samples is designed to exceed the maximum PLC channel delay spread (L_h), which is inserted at the beginning of each OFDM symbol by copying the last N_{CP} samples of the IFFT output $\mathbf{x}$ and appending them at the beginning of $\mathbf{x}$ to produce the transmitted symbol $\tilde{\mathbf{x}}$ of length $N_t = N + N_{CP}$ samples expressed as $\tilde{\mathbf{x}} = [x_{N-N_{CP}}, x_{N-N_{CP}+1}, \ldots, x_{N-1}, x_0, x_1, \ldots, x_{N-1}]$.

The frequency response, $H(f)$, of the PLC channel exhibiting L propagation paths can be modelled using Zimmermann and Dostert model as [1]–[3], [10]

$$H(f) = \sum_{i=1}^{L} \underbrace{g_i}_{\text{weighting}} \underbrace{e^{-(a_0+a_1 f^k)d_i}}_{\text{attenuation}} \underbrace{e^{-j2\pi f \frac{d_i}{v_p}}}_{\text{delay}}, \tag{2}$$

where g_i is the weighting factor, a_0 and a_1 are the attenuation parameters, $k \in [0.5, 1]$ is the exponent of the attenuation factor, d_i is the path length and $\frac{d_i}{v_p} = \tau_i$ is the path propagation delay, where v_p is the phase velocity of the wave. The validity of Zimmermann and Dostert model has been checked by the Alternative Transients Program-Electromagnetic Transients Program (ATP-EMTP) [1]. It has been found that the amplitude for the Zimmermann and Dostert model and that predicted by ATP-EMTP software are similar, while the time delay in the Zimmermann and Dostert model and ATP-EMTP software is different. Therefore, the time delay problem in Zimmermann and Dostert model has been re-solved by utilizing the modified Zimmermann and Dostert model, which removes the distance parameter d_i in the attenuation term to achieve matching results to the ATP-EMTP software [1].

Under perfect synchronization conditions, the received signal $\tilde{y}_n$ in the time domain can be expressed as:

$$\tilde{y}_n = \sum_{i=0}^{L_h-1} h_i \tilde{x}_{n-i} + \lambda_n, \quad 0 \leq n \leq N + N_{CP} - 1. \tag{3}$$

where $\{h_i\}_{i=0}^{L_h-1}$ are the coefficients of the discrete impulse response of the multipath PLC channel in the time domain, L_h is the channel length and $\boldsymbol{\lambda} = [\lambda_0, \lambda_1, \ldots, \lambda_{N+N_{CP}-1}]$ denotes the total non-Gaussian noise samples in the time domain that's include the BI and BGM. λ_n can be expressed as $\lambda_n = \tilde{b}_n + i_n$, where $\tilde{b}_n$ is BI and i_n is BGM. The real and imaginary components of the BI can be expressed as $\tilde{b}_n^{\Re} = b_n \cos(\theta_n)$ and $\tilde{b}_n^{\Im} = b_n \sin(\theta_n)$, respectively. Moreover, we assume that the PLC channel characteristics will not change over time. The only time-varying parameter in the PLC channel is the impulsive noise and background interference noise samples. However, the statistics of these two types of noise are assumed fixed. Furthermore, for the frequency response of the PLC channel we are using the standard 15-path channel with constant parameters as tabulated in Table I [2].

In order to reduce the effects of impulsive noise in the time domain, an impulsive noise mitigation method based on a blanking non-linearity is applied before the OFDM demodulator, replacing the incoming signal $\tilde{y}_n$ in (3) by a zero value when the complex received signal magnitudes exceed a blanking threshold [15], [25] as

$$r_n = \begin{cases} \tilde{y}_n & \text{if } |\tilde{y}_n| \leq T_b \\ 0, & \text{otherwise ,} \end{cases} \quad n = 0, 1, \cdots, N-1, \tag{4}$$

where T_b is the blanking threshold. We utilize this threshold derived in [26] for the real and imaginary parts of 4096-QAM modulation. It is worth highlighting that this threshold is optimal for real-valued OFDM signals, however, when using the blanker on the real and imaginary parts separately, the threshold may be suboptimal.

III. THE EFFECTIVE NOISE PDFs DERIVATION AT THE ZF EQUALIZER OUTPUT

Assuming perfect time synchronization condition between the transmitter and the receiver, the received signal after CP removal, $\mathbf{y} = [y_0, y_1, \ldots, y_{N-1}]$, and FFT operation for all FFT sub-carriers $k = 0, 1, \ldots, N-1$ can be expressed as

$$Y_k = \frac{1}{\sqrt{N}} \sum_{n=0}^{N-1} y_n e^{\frac{-j2\pi nk}{N}} = H_k X_k + \Lambda_k, \tag{5}$$

where $\Lambda_k = \frac{1}{\sqrt{N}} \sum_{n=0}^{N-1} \lambda_n e^{\frac{-j2\pi nk}{N}}$ represents the FFT of the total non-Gaussian noise samples λ_n, X_k represents the modulated symbols, and H_k denotes the complex frequency response of the modified PLC channel for the k-th FFT sub-carrier. The magnitude $|H_k| = \sqrt{(H_k^{\Re})^2 + (H_k^{\Im})^2}$ exhibits a Rayleigh distribution of two degrees of freedom [1], i.e.

$$p_H(|H_k|) = \frac{|H_k|}{\sigma_h^2} e^{\left(\frac{-|H_k|^2}{2\sigma_h^2}\right)}, \quad |H_k| \geq 0, \tag{6}$$

and the phase, $\phi = \tan^{-1}\left(\frac{H_k^{\Im}}{H_k^{\Re}}\right)$, is uniformly distributed as

$$p_\phi(\phi) = \frac{1}{2\pi} \quad \text{for} \quad -\pi \leq \phi < \pi, \tag{7}$$

where $H_k^{\Re}$ and $H_k^{\Im}$ are zero-mean statistically independent orthogonal Gaussian random variables and their variances are $\sigma_h^2 = \frac{1}{2}$ per dimension.

The transmitted data symbols can be recovered by utilizing a ZF equalizer after the N-point FFT operation in (5) as

$$C_k^{\text{ZF}} Y_k = X_k + C_k^{\text{ZF}} \Lambda_k, \tag{8}$$

where $\hat{Y}_k = C_k^{\text{ZF}} Y_k = \frac{Y_k^{\Re} + jY_k^{\Im}}{H_k^{\Re} + jH_k^{\Im}}$ is the complex-valued equalized received signal, $C_k^{\text{ZF}} = \frac{1}{H_k^{\Re} + jH_k^{\Im}}$ are the complex-valued of the ZF equalizer, and $C_k^{\text{ZF}} \Lambda_k = Z_k = \frac{\Lambda_k^{\Re} + j\Lambda_k^{\Im}}{H_k^{\Re} + jH_k^{\Im}}$ are the complex-valued equalized non-Gaussian noise samples.

A. Nakagami-m Background Interference (BI) Noise

In the presence of Nakagami-m BI, λ_n in (3) can be expressed as $\lambda_n = \lambda_n^{\Re} + j\lambda_n^{\Im}$, where $\lambda_n^{\Re} = \tilde{b}_n^{\Re}$ and $\lambda_n^{\Im} = \tilde{b}_n^{\Im}$ are the real and imaginary components of BI, respectively. Practically, the envelope b_n of BI in the time-domain follows the Nakagami-m distribution and it can be expressed as [5]

$$p(b_n) = \frac{2b_n^{2m-1}}{\Gamma(m)} \left(\frac{m}{\Omega}\right)^m e^{-\left(\frac{mb_n^2}{\Omega}\right)}, \tag{9}$$

where $m = (\mathbb{E}\{b_n^2\})^2/\mathbb{E}\{(b_n^2 - \mathbb{E}\{b_n^2\})^2\}$ is the Nakagami-m parameter, which denotes the closeness between the Nakagami and Rayleigh PDFs, $\Omega = \mathbb{E}\{b_n^2\}$ is the mean power of the random variable b_n, $\Gamma(\cdot)$ is the Gamma function, and $\mathbb{E}\{\cdot\}$ is the expectation value. Moreover, the phase θ_n is uniformly distributed in $[-\pi, \pi)$. Thus, the distribution of $\lambda_n^{\Re}$ conditioned on θ_n, $p_\lambda(\lambda_n^{\Re}|\theta_n)$, can be expressed as [5]

$$p_\lambda(\lambda_n^{\Re}|\theta_n) = \frac{2(\lambda_n^{\Re})^{2m-1}}{\Gamma(m)\cos^{2m}(\theta_n)} \left(\frac{m}{\Omega}\right)^m e^{\left(\frac{-m(\lambda_n^{\Re})^2}{\Omega\cos^2(\theta_n)}\right)}, \tag{10}$$

while the distribution of $p_\lambda(\lambda_n^{\Im}|\theta_n)$ can be defined as

$$p_\lambda(\lambda_n^{\Im}|\theta_n) = \frac{2(\lambda_n^{\Im})^{2m-1}}{\Gamma(m)\sin^{2m}(\theta_n)} \left(\frac{m}{\Omega}\right)^m e^{\left(\frac{-m(\lambda_n^{\Im})^2}{\Omega\sin^2(\theta_n)}\right)}, \tag{11}$$

The closed-form expressions of the real part distribution, $p_\lambda(\lambda_n^{\Re})$, utilizing (10) and the imaginary part distribution, $p_\lambda(\lambda_n^{\Im})$, utilizing (11) for $0 < m < 1$, $m \neq \frac{1}{2}$ and $-\infty < \lambda_n^r < \infty$, can be expressed as [7]

$$\begin{aligned} p_\lambda(\lambda_n^r) = \frac{e^{-\frac{m(\lambda_n^r)^2}{\Omega}}}{\sqrt{\pi}\Gamma(m)}\sqrt{\frac{m}{\Omega}}\Bigg[\frac{\Gamma(\frac{1}{2}-m)}{\Gamma(1-m)}\left(\frac{m(\lambda_n^r)^2}{\Omega}\right)^{m-\frac{1}{2}} \times \\ {}_1F_1\left(\frac{1}{2}, \frac{1}{2}+m, \frac{m(\lambda_n^r)^2}{\Omega}\right) + \frac{\Gamma(m-\frac{1}{2})}{\sqrt{\pi}} \times \\ {}_1F_1\left(1-m, \frac{3}{2}-m, \frac{m(\lambda_n^r)^2}{\Omega}\right)\Bigg], \end{aligned} \tag{12}$$

and for $m = \frac{1}{2}$ as

$$p_\lambda(\lambda_n^r) = \frac{1}{\pi}\sqrt{\frac{1}{2\pi\Omega}}e^{-\frac{(\lambda_n^r)^2}{4\Omega}}K_0\left(\frac{(\lambda_n^r)^2}{4\Omega}\right), \tag{13}$$

where $r = \{\Re, \Im\}$, ${}_1F_1(a;b;z)$ is the confluent hypergeometric function expressed as [27, Eq.(9.210[10])] and $K_0(\cdot)$ is the modified Bessel function of the second kind of order zero.

After performing the FFT operation in (5), the distribution of Nakagami-m BI samples in (12) and (13) will be changed and we can determine it using a statistical approximation. According to the Central Limit Theorem (CLT), the PDF of the real and imaginary parts of BI, $p_\lambda(\lambda_n^r)$, after performing the FFT operation will be approaching the normal distribution [5], i.e. $p_B(B_k^r) = \mathcal{N}(B_k^r, \mu_b, \sigma_b^2) = \frac{1}{\sqrt{2\pi}\sigma_b}\exp\left(-\frac{(B_k^r-\mu_b)^2}{2\sigma_b^2}\right)$ with mean $\mu_b = 0$ and the variance σ_b^2. In this case, σ_b^2 can be computed from (12) or (13), which gives equal variance. For simplicity, σ_b^2 can be computed from (13) utilizing the integral formula in [27, Eq.(6.621,3)] as

$$\begin{aligned}\sigma_b^2 &= \mathbb{E}\{(\lambda_n^r)^2\} - (\mathbb{E}\{\lambda_n^r\})^2 \\ &= \frac{2\Omega}{\pi}\left(\Gamma\left(\frac{3}{2}\right)\right)^2 {}_2F_1\left(\frac{3}{2}, \frac{1}{2}, 2, 0\right),\end{aligned} \tag{14}$$

where σ_b^2 depends on the mean power of the random variable b_n, $\Omega = \mathbb{E}\{b_n^2\}$ and ${}_2F_1(a, b; c; z)$ is the Gauss hypergeometric function expressed as [27, Eq.(9.14)].

The joint PDF of the real and imaginary components can be expressed as $p_B(B_k^\Re, B_k^\Im) = p_B(B_k^\Re)p_B(B_k^\Im) = \mathcal{N}(B_k^\Re, 0, \sigma_b^2)\mathcal{N}(B_k^\Im, 0, \sigma_b^2)$. Therefore, the magnitude $|B_k| = \sqrt{(B_k^\Re)^2 + (B_k^\Im)^2}$ follows a Rayleigh distribution and its phase $\phi_{B_k} = \tan^{-1}\left(\frac{B_k^\Im}{B_k^\Re}\right)$ exhibits a uniform distribution in $[-\pi, \pi)$. Hence, the complex-valued noise samples after the ZF equalizer in (8) can be expressed as

$$Z_k = Z_k^\Re + jZ_k^\Im = \frac{|B_k|e^{j\phi_{B_k}}}{|H_k|e^{j\phi_{H_k}}} = \chi_k e^{j\left(\phi_{B_k} - \phi_{H_k}\right)}, \tag{15}$$

where $Z_k^\Re = \chi_k\cos(\phi_{t_k})$ and $Z_k^\Im = \chi_k\sin(\phi_{t_k})$ are the real and imaginary parts of the equalized noise samples, respectively, and $\phi_{t_k} = \phi_{B_k} - \phi_{H_k}$ is the total phase. Thus, the PDF of $\chi_k = \frac{|B_k|}{|H_k|}$

can be computed as a ratio of two random variables with Rayleigh distributions. The joint PDF between B_k and H_k can be expressed as [28]

$$p_{BH}(|B_k|,|H_k|) = \frac{|B_k||H_k|}{\sigma_b^2\sigma_h^2} e^{-\frac{|B_k|^2}{2\sigma_b^2}-\frac{|H_k|^2}{2\sigma_h^2}}, \tag{16}$$

substituting $|B_k| = \chi_k|H_k|$ in (16), we get

$$p_{BH}(\chi_k|H_k|,|H_k|) = \frac{\chi_k|H_k|^2}{\sigma_b^2\sigma_h^2} e^{-|H_k|^2\left(\frac{\sigma_h^2|\chi_k|^2+\sigma_b^2}{2\sigma_b^2\sigma_h^2}\right)}, \tag{17}$$

we have utilized the computational knowledge engine[1] to determine the PDF of χ_k using the division of two random variables formula [28], yield

$$\begin{aligned} p_{\chi_k}(\chi_k) &= \int_0^\infty \frac{\chi_k|H_k|^3}{\sigma_b^2\sigma_h^2} e^{-|H_k|^2\left(\frac{\sigma_h^2|\chi_k|^2+\sigma_b^2}{2\sigma_b^2\sigma_h^2}\right)} dH_k \\ &= \frac{2\sigma_h^2\sigma_b^2\chi_k}{(\sigma_h^2|\chi_k|^2+\sigma_b^2)^2}, \text{ for } \Re\left(\frac{\sigma_h^2|\chi_k|^2+\sigma_b^2}{2\sigma_b^2\sigma_h^2}\right) > 0. \end{aligned} \tag{18}$$

The total phase ϕ_{t_k} is uniformly distributed over $[-\pi,\pi)$ as $p_\phi(\phi_{t_k}) = \frac{1}{2\pi}$. Thus, the conditional PDF of $p_Z(Z_k^\Re|\phi_{t_k})$ of the real part can be expressed as

$$\begin{aligned} p_Z(Z_k^\Re|\phi_{t_k}) &= \frac{1}{|\cos(\phi_{t_k})|} p(\chi_k)\Big|_{\chi_k = Z_k^\Re/\cos(\phi_{t_k})} \\ &= \frac{1}{|\cos^2(\phi_{t_k})|} \frac{2\sigma_h^2\sigma_b^2 Z_k^\Re}{(\sigma_h^2|\frac{Z_k^\Re}{\cos(\phi_{t_k})}|^2+\sigma_b^2)^2}, \end{aligned} \tag{19}$$

and the joint PDF, $p_{Z,\phi}(Z_k^\Re,\phi_{t_k})$, can be expressed as

$$\begin{aligned} p_{Z,\phi}(Z_k^\Re,\phi_{t_k}) &= p_Z(Z_k^\Re|\phi_{t_k})p_\phi(\phi_{t_k}) \\ &= \frac{1}{2\pi}\frac{1}{|\cos^2(\phi_{t_k})|} \frac{2\sigma_h^2\sigma_b^2 Z_k^\Re}{(\sigma_h^2|\frac{Z_k^\Re}{\cos(\phi_{t_k})}|^2+\sigma_b^2)^2}. \end{aligned} \tag{20}$$

Hence, the $p(Z_k^\Re)$ of the effective noise samples after ZF equalization can be computed as

$$\begin{aligned} p_Z(Z_k^\Re) &= \int_{-\pi}^{\pi} p_{Z,\phi}(Z_k^\Re,\phi_{t_k}) d\phi_{t_k} \\ &= 4\int_0^{\pi/2} \frac{1}{\pi|\cos^2(\phi_{t_k})|} \frac{\sigma_h^2\sigma_b^2 Z_k^\Re}{(\sigma_h^2|\frac{Z_k^\Re}{\cos(\phi_{t_k})}|^2+\sigma_b^2)^2} d\phi_{t_k}, \end{aligned} \tag{21}$$

[1]https://www.wolframalpha.com

assuming $\cos^2(\phi_{t_k}) = t$ gives $d\phi_{t_k} = -\frac{dt}{2\sqrt{t}\sqrt{1-t}}$, then

$$p_Z(Z_k^{\Re}) = 2\int_0^1 \frac{\sigma_h^2\sigma_b^2 Z_k^{\Re}\sqrt{t}}{\pi\sqrt{1-t}(\sigma_h^2|Z_k^{\Re}|^2 + \sigma_b^2 t)^2}dt, \tag{22}$$

utilizing the computational knowledge engine[1], we get

$$p_Z(Z_k^{\Re}) = \frac{\sigma_b^2\sigma_h}{2\left(\sigma_h^2|Z_k^{\Re}|^2 + \sigma_b^2\right)^{\frac{3}{2}}}. \tag{23}$$

It is worth noting that $p_Z(Z_k^{\Re}) = p_Z(Z_k^{\Im})$.

B. Impulsive Noise

In the presence of BGM, $\lambda_n^{\Re} = i_n^{\Re}$ and $\lambda_n^{\Im} = i_n^{\Im}$ in (3), where $i_n^{\Re}$ and $i_n^{\Im}$ are the real and imaginary parts of the Bernoulli Gaussian mixture (BGM) model represent the mixture of impulsive noise and background Gaussian noise due to thermal effects in the electronics in the time domain. Their PDFs can be expressed as a sum of two Gaussian PDFs as [9], [10], [15], [24]

$$p(\lambda_n^r) = (1-\alpha)\mathcal{N}(\lambda_n^r, 0, \sigma_w^2) + \alpha\mathcal{N}(\lambda_n^r, 0, \sigma_w^2 + \sigma_i^2), \tag{24}$$

where $0 < \alpha < 1$ is the probability of impulse occurrence, σ_w^2 and σ_i^2 are the AWGN and impulsive noise variances, respectively. The FFT operation in (5) will spread the effect of the impulsive noise on each subcarrier converting its PDF to a Gaussian distribution, thus, the PDF in (24) can be expressed as [9], [24]

$$p_\Lambda(\Lambda_k^r) = \sum_{n=0}^{N}\binom{N}{n}\alpha^n(1-\alpha)^{N-n}\mathcal{N}(\Lambda_k^r, 0, \sigma_n^2), \tag{25}$$

where $\sigma_n^2 = \sigma_w^2 + \frac{n\sigma_i^2}{N}$ and $\binom{N}{n} = \frac{N!}{(N-n)!n!}$. It is easy to show the magnitude of impulsive noise after FFT operation, $|\Lambda_k| = \sqrt{(\Lambda_k^{\Re})^2 + (\Lambda_k^{\Im})^2}$, exhibits weighted sum of Rayleigh distributions expressed as

$$p_\Lambda(|\Lambda_k|) = \sum_{n=0}^{N}\binom{N}{n}\alpha^n(1-\alpha)^{N-n}\frac{|\Lambda_k|}{\sigma_n^2}e^{-\frac{|\Lambda_k|^2}{2\sigma_n^2}}, \tag{26}$$

and its phase $\phi_{\Lambda_k} = \tan^{-1}\left(\frac{\Lambda_k^{\Im}}{\Lambda_k^{\Re}}\right)$ exhibits a uniform distribution in $[-\pi, \pi)$ as $p_\phi(\phi_{\Lambda_k}) = \frac{1}{2\pi}$. Thus, the PDF of the effective noise samples at the ZF output can be expressed as

$$Z_k = \sum_{n=0}^{N} \binom{N}{n} \alpha^n (1-\alpha)^{N-n} \frac{|\Lambda_k| e^{j\phi_{\Lambda_k}}}{|H_k| e^{j\phi_{H_k}}} = \chi_k e^{j\phi_{t_k}}, \tag{27}$$

following similar derivation steps in (19)-(23), we obtain

$$p_Z(Z_k^r) = \sum_{n=0}^{N} \binom{N}{n} \frac{\alpha^n (1-\alpha)^{N-n} \sigma_n^2 \sigma_h}{2\left(\sigma_h^2 |Z_k^r|^2 + \sigma_n^2\right)^{\frac{3}{2}}}. \tag{28}$$

C. Combined BI and BGN

In the presence of the combined BI and BGN, $\lambda_n^{\Re} = \tilde{b}_n^{\Re} + i_n^{\Re} = \left(b_n \cos(\theta_n) + i_n^{\Re}\right)$ and $\lambda_n^{\Im} = \tilde{b}_n^{\Im} + i_n^{\Im} = \left(b_n \sin(\theta_n) + i_n^{\Im}\right)$ are the real and imaginary components of the overall non-Gaussian noise samples in (3), respectively. The complex-valued noise samples after FFT operation in (5) can be expressed as $\xi_k = \xi_k^{\Re} + j\xi_k^{\Im} = (B_k^{\Re} + \Lambda_k^{\Re}) + j(B_k^{\Im} + \Lambda_k^{\Im})$. Hence, the joint PDF, $p(B_k^r, \Lambda_k^r)$, can be expressed as

$$p_{B,\Lambda}(B_k^r, \Lambda_k^r) = \sum_{n=0}^{N} \binom{N}{n} \frac{\alpha^n (1-\alpha)^{N-n}}{2\pi\sigma_b\sigma_n} e^{-\frac{(B_k^r)^2}{2\sigma_b^2} - \frac{(\Lambda_k^r)^2}{2\sigma_n^2}}. \tag{29}$$

Assuming $\xi_k^r = B_k^r + \Lambda_k^r$ and substituting $\Lambda_k^r = \xi_k^r - B_k^r$ in (29), the $p(\xi_k^r)$ can be computed utilizing [28] as

$$\begin{aligned} p_\xi(\xi_k^r) = \int_{-\infty}^{\infty} \sum_{n=0}^{N} \binom{N}{n} \alpha^n (1-\alpha)^{N-n} \frac{e^{-\frac{|\xi_k^r|^2}{2\sigma_b^2}}}{2\pi\sigma_b\sigma_n} \\ \times e^{-(B_k^r)^2\left(\frac{1}{2\sigma_b^2} + \frac{1}{2\sigma_n^2}\right) + B_k^r \frac{|\xi_k^r|}{\sigma_b^2}} dB_k^r. \end{aligned} \tag{30}$$

Comparing (30) with the integral formula in [27, Eq.$(3.462, 2.^8)$], we can obtain the distribution of the combined noise samples after the FFT operation as

$$p_\xi(\xi_k^r) = \sum_{n=0}^{N} \binom{N}{n} \alpha^n (1-\alpha)^{N-n} \frac{e^{-\frac{(\xi_k^r)^2}{2(\sigma_b^2+\sigma_n^2)}}}{\sqrt{2\pi(\sigma_b^2+\sigma_n^2)}}. \tag{31}$$

Hence, the PDF of the magnitude of ξ_k, can be described by a weighted sum of Rayleigh PDFs as

$$p_{\xi}(|\xi_k|) = \sum_{n=0}^{N} \binom{N}{n} \frac{\alpha^n (1-\alpha)^{N-n} |\xi_k|}{\sigma_b^2 + \sigma_n^2} e^{-\frac{|\xi_k|^2}{2(\sigma_b^2+\sigma_n^2)}}, \tag{32}$$

and its phase can be described by a uniform distribution as $p_{\phi}(\phi_{\xi_k}) = \frac{1}{2\pi}$. Thus, the effective noise samples after the ZF equalizer can be expressed as in (27) by utilizing $|\xi_k| e^{j\phi_{\xi_k}}$ instead of $|\Lambda_k| e^{j\phi_{\Lambda_k}}$ and following similar derivation steps as described in (19)-(23), we get

$$p_Z(Z_k^r) = \sum_{n=0}^{N} \binom{N}{n} \frac{\alpha^n (1-\alpha)^{N-n} \sigma_h (\sigma_b^2 + \sigma_n^2)}{2\big(\sigma_h^2 |Z_k^r|^2 + (\sigma_b^2 + \sigma_n^2)\big)^{\frac{3}{2}}}. \tag{33}$$

IV. Maximum Likelihood (ML) detector, log-likelihood ratio (LLR) and BER derivations

A. ML Detector and LLR Derivation

We proceed now to compute the likelihood based on maximum likelihood (LML) detector as in [13]. For the case of BI only utilizing (23), the LML with respect to M-ary QAM $\forall k = 0, 1, \cdots \frac{N-1}{\log_2(M)}$ can be expressed as

$$\frac{\sum_{X_k \in \mathcal{M}^r(0)} \frac{1}{\left(\sigma_h^2 |\hat{Y}_k^r - X_k|^2 + \sigma_t^2\right)^{\frac{3}{2}}}}{\sum_{X_k \in \mathcal{M}^r(1)} \frac{1}{\left(\sigma_h^2 |\hat{Y}_k^r - X_k|^2 + \sigma_t^2\right)^{\frac{3}{2}}}} \underset{1}{\overset{0}{\gtrless}} 1, \tag{34}$$

moreover, the LML detector in case of BGM utilizing (28) and combined BI and BGM utilizing (33) can be expressed as

$$\frac{\sum_{X_k \in \mathcal{M}^r(0)} \sum_{n=0}^{N} \binom{N}{n} \frac{\alpha^n (1-\alpha)^{N-n}}{\left(\sigma_h^2 |\hat{Y}_k^r - X_k|^2 + \sigma_t^2\right)^{\frac{3}{2}}}}{\sum_{X_k \in \mathcal{M}^r(1)} \sum_{n=0}^{N} \binom{N}{n} \frac{\alpha^n (1-\alpha)^{N-n}}{\left(\sigma_h^2 |\hat{Y}_k^r - X_k|^2 + \sigma_t^2\right)^{\frac{3}{2}}}} \underset{1}{\overset{0}{\gtrless}} 1, \tag{35}$$

where $\sigma_t^2 = \sigma_b^2$, $\sigma_t^2 = \sigma_n^2$ and $\sigma_t^2 = \sigma_b^2 + \sigma_n^2$ for the cases of BI, BGM and combined noise, respectively. $\mathcal{M}^r(0)$ and $\mathcal{M}^r(1)$ denote the signal subset of all possible equiprobable symbols of X_k being 0 or 1, respectively. Furthermore, the Sum-Product Algorithm (SPA) adopted in this paper for irregular LDPC decoder can be improved utilizing the LLRs computed based on the

LML detector for each coded bit of the received signal. Thus, the modified initial LLRs, L_k^r, can be expressed as

$$L_k^r = \log \frac{\sum_{X_k \in \mathcal{M}^r(0)} p_Z(\hat{Y}_k^r | X_k)}{\sum_{X_k \in \mathcal{M}^r(1)} p_Z(\hat{Y}_k^r | X_k)}. \tag{36}$$

B. BER Derivation

We proceed now to compute the SER employing the LLR based on ML detector in (36). For the case of BGM and combined BI and BGM, we can derived the SER using the cumulative distribution function (CDF) as

$$\begin{aligned} F_z(z) &= \int_{-\infty}^{z} \sum_{n=0}^{N} \binom{N}{n} \alpha^n (1-\alpha)^{N-n} \frac{\sigma_h \sigma_t^2}{2(\sigma_h^2 u^2 + \sigma_t^2)^{\frac{3}{2}}} du \\ &= \sum_{n=0}^{N} \binom{N}{n} \alpha^n (1-\alpha)^{N-n} \left[\frac{1}{2} + \frac{\sigma_h z}{2(\sigma_h^2 z^2 + \sigma_t^2)^{\frac{1}{2}}} \right], \end{aligned} \tag{37}$$

hence, the SER, $P_s^{4-\mathrm{QAM}} = F_z(0)$, can be computed as

$$P_s^{4-\mathrm{QAM}} = \sum_{n=0}^{N} \binom{N}{n} \alpha^n (1-\alpha)^{N-n} \left[1 - \sqrt{\frac{\psi}{\psi+1}} \right], \tag{38}$$

where $\psi = \frac{E_b \sigma_h^2}{\sigma_t^2}$ and E_s is the energy per transmitted symbol. Thus, the SER of the M-ary QAM signal for $M >> 4$ can be derived using the SER of the $\sqrt{M}$-ary pulse amplitude modulation (PAM) as

$$P_s^{\sqrt{M}-\mathrm{PAM}} = \left(1 - \frac{1}{\sqrt{M}} \right) \sum_{n=0}^{N} \binom{N}{n} \alpha^n (1-\alpha)^{N-n} (1-\Psi), \tag{39}$$

and in case of BI only can be derived as

$$P_s^{\sqrt{M}-\mathrm{PAM}} = \left(1 - \frac{1}{\sqrt{M}} \right) (1-\Psi), \tag{40}$$

where $\Psi = \sqrt{\frac{K\psi}{K\psi+1}}$ and $K = \frac{3\log_2(M)}{2(M-1)}$. Therefore, the general expression formula that describes the tight approximation of BER in different scenarios of BI, BGM and their combination over PLC channel utilizing M-ary QAM constellation can be expressed as [13]

$$P_b^{M-\mathrm{QAM}} \approx \frac{1 - \left(1 - P_s^{\sqrt{M}-\mathrm{PAM}} \right)^2}{\log_2(M)}. \tag{41}$$

Moreover, the Stirlings logarithmic factorial approximation, $\log(f!) = \left(f + \frac{1}{2}\right)\log(f) - f + \frac{1}{2}\log(2\pi)$ [29], is used to compute the large factorials in (28), (33), (35), (38) and (39).

V. EXIT CHART ANALYSIS

EXtrinsic Information Transfer (EXIT) chart analysis was first introduced in [21] to analyze the convergence of an iterative decoding, which can be achieved by observing the mutual information exchange between the variable node processors (VNPs) and check node processors (CNPs) that work cooperatively and iteratively to make the bit decisions in the iterative LDPC decoder [21], [30]. In case of combined BI and BGM, the LLR values of $\mathcal{C}^{\mathrm{BPSK}}$ constellation can be computed using (36) utilized $p_Z(\hat{Y}_k^{\Re}|X_k = \pm 1)$ in (33). Due to the hard simplification of the LLR equation in this case, we simplify the magnitude PDF of the total noise sample in (31) after the FFT-OFDM demodulator to new formula as

$$p_{\xi}(\xi_k^r) = \frac{1}{\sqrt{2\pi(\sigma_b^2 + \sigma_t^2)}} \exp\left(-\frac{(\xi_k^r)^2}{2(\sigma_b^2 + \sigma_t^2)}\right), \tag{42}$$

where the total noise variance at the OFDM receiver due to BGM can be expressed as $\sigma_t^2 = \sigma_w^2 + \alpha\sigma_i^2 = \sigma_w^2(1 + \alpha\rho)$ and $\rho = \frac{\sigma_i^2}{\sigma_w^2}$ is the impulsive to Gaussian noise power ratio. Moreover, we can approximate the equalized noise sample in (33) to new PDF utilizing (42) with variance $\frac{(\sigma_b^2+\sigma_t^2)}{\sigma_h^2}$ as

$$p_Z(Z_k^r) = \frac{\sigma_h}{\sqrt{2\pi(\sigma_b^2 + \sigma_t^2)}} \exp\left(-\sigma_h^2\frac{(Z_k^r)^2}{2(\sigma_b^2 + \sigma_t^2)}\right), \tag{43}$$

hence, the LLR values utilizing (43) can be computed as

$$L_k^A = \frac{p_Z(\hat{Y}_k^{\Re}|X_k = -1)}{p_Z(\hat{Y}_k^{\Re}|X_k = +1)} = \frac{2\sigma_h^2}{(\sigma_b^2 + \sigma_t^2)}\hat{Y}_k^{\Re}. \tag{44}$$

Note that L_k^A conditioned on $X_k = \pm 1$ has mean value, $\mu_A = \pm\frac{2\sigma_h^2}{(\sigma_b^2+\sigma_t^2)}$, and variance, $\sigma_A^2 = \frac{4\sigma_h^2}{(\sigma_b^2+\sigma_t^2)}$ [21]. Fig. 2 represent plots of the mutual information $I_A = J(\sigma_A)$ as a function of σ_A using [30, Eq.12] utilizing the derived PDF in (44) versus the I_A utilizing the derivation of S.

Brink in [21]. It can be noted that I_A is proportional to σ_A^2 and inversely proportional to σ_b^2 and σ_t^2. Moreover, the derived system in the presence of the non-Gaussian noise reaches the maximum I_A faster than the conventional system due to the achieved lower σ_A^2 in the case of combined BI and BGM.

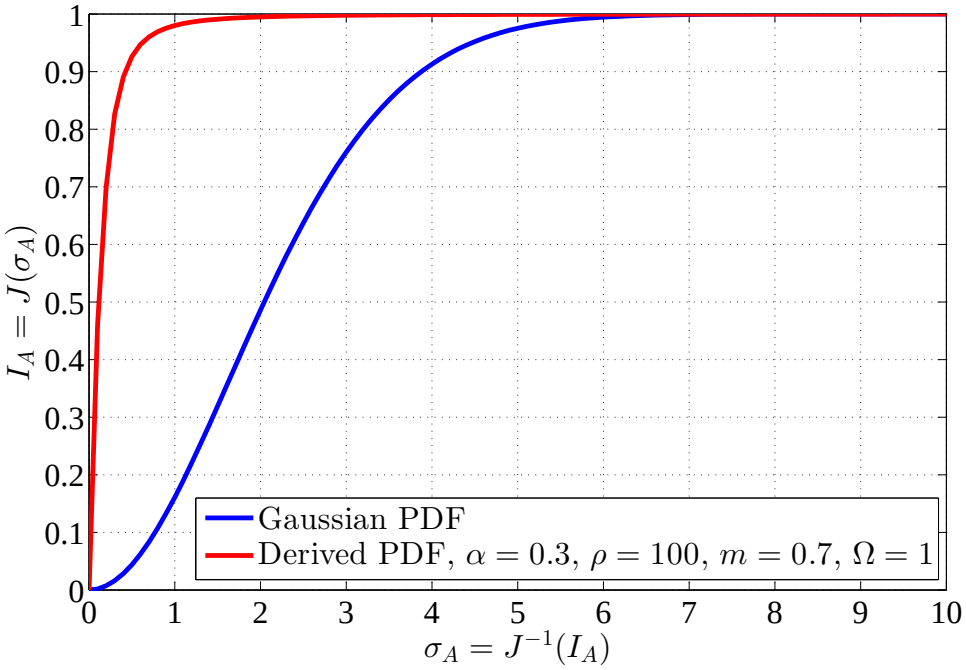

Fig. 2. Comparison of mutual information between S. Brink derivation over AWGN channel in [21] and the derived PDF over PLC channel.

Thus, the EXIT functions of irregular LDPC codes involving all variable nodes d_v and all check nodes d_c can be expressed as [21]

$$I_{E,V}\left(I_{A,V}\right) = \sum_{i=1}^{d_v} \epsilon_i J\left(\sqrt{\left(d_v - 1\right)\left[J^{-1}(I_{A,V})\right]^2 + \sigma_A^2}\right),$$
$$I_{E,C}(I_{A,C}) = 1 - \sum_{i=1}^{d_c} \varepsilon_i J\left(\sqrt{\left(d_c - 1\right)\left[J^{-1}(1 - I_{A,C})\right]^2}\right), \quad (45)$$

where ϵ_i and ε_i are the fractions of degree i of variable nodes and check nodes, respectively. For computer implementation, we approximate $I_A = J(\sigma_A)$ in Fig. 2 into three regions using

least-square curve fitting [31] as

$$J(\sigma_A) = \begin{cases} 1 - 0.9949e^{-5.917}, & 0 \leq \sigma_A \leq 0.4 \\ 1 - 0.375e^{-3.159}, & 0.4 < \sigma_A \leq 1 \\ 1 - 0.05729e^{-1.161}, & 1 < \sigma_A \leq 10 \end{cases} \tag{46}$$

and the inverse function $\sigma_A = J^{-1}(I_A)$ can be computed as

$$J^{-1}(I_A) = \begin{cases} -\frac{1}{5.917} \ln\left(\frac{1-I_A}{0.9949}\right), & 0 < I_A \leq 0.9067 \\ -\frac{1}{3.159} \ln\left(\frac{1-I_A}{0.375}\right), & 0.9067 < I_A \leq 0.9841 \\ -\frac{1}{1.161} \ln\left(\frac{1-I_A}{0.05729}\right), & 0.9841 < I_A \leq 1. \end{cases} \tag{47}$$

VI. SIMULATION RESULTS

In this Section, we investigate the exact fitting of the derived distributions by simulation. Fig. 3 illustrates the histogram plots of the real part of the received signal over the 15-path PLC channel, where the channel parameters are listed in Table I [2], in the presence of the BI only with $\Omega = 1$ and $m = 0.7$ utilizing (23), BGM only with $\alpha = 0.3$ and $\rho = 100$ utilizing (28), and their combination utilizing (33) at the output of the ZF equalizer. It is worth noting that the derivations of theoretical, closed-form PDFs exhibit close matching with their corresponding empirically obtained distributions using Monte-Carlo simulation. The mean squared error (MSE), which can be evaluated as $\mathrm{MSE} = \frac{1}{N}\sum_{n=1}^{N}(\hat{Y}_n^{\Re} - Y_n^{\Re})^2$ is obtained as $4.21 \times 10^{-12}, 5.47 \times 10^{-10}$ and 1.11×10^{-11} for the BI, BGM and combined BI and BGM, respectively.

In order to assess the performance of the proposed LDPC-COFDM system over the PLC channel contaminated by different scenarios of BI and BGM, the derived PDFs are utilized. The simulation parameters were set as follows, the number of sub-carriers chosen as $N = 4096$, modulated using a 4096-QAM constellation for a rate-$1/2$ irregular LDPC code. Each code block is decoded by using SPA with the maximum number of iterations 50. The PLC is modelled by modified the Zimmermann model for 15-taps. The system performance is compared against

TABLE I

PARAMETERS OF THE 15-PATH MODEL

Attenuation parameters					
$k = 1$		$a_0 = 0$		$a_1 = 2.5 \times 10^{-9}$	
Path-parameters					
i	g_i	$d_i(m)$	i	g_i	$d_i(m)$
1	0.029	90	9	0.071	411
2	0.043	102	10	-0.035	490
3	0.103	113	11	0.065	567
4	-0.058	143	12	-0.055	740
5	-0.045	148	13	0.042	960
6	-0.040	200	14	-0.059	1130
7	0.038	260	15	0.049	1250
8	-0.038	322			

the conventional LDPC-COFDM system, in which a blanking non-linearity impulsive noise mitigation method is utilize (4), and the LLRs are computed based on the Gaussian distribution. Additionally, both systems are compared to the uncoded system that utilizes LLR computed based on the LML detector and for the frequency bandwidth of 22.4 MHz that utilize in HomePlug AV [12].

In Fig. 4-(a), we demonstrate the BER performance of LDPC-COFDM system utilizing the derived PDF in the presence of Nakagami-m BI only with $m = 0.7$ and 0.5, in which the obtained LLRs are computed based on the derived PDF in (23). This performance is compared to the conventional system and uncoded system, respectively. It can be seen from the figure that the BER performance is approximately unaffected by changes in the value of m associated to Nakagami distribution. This is due to the fact that the BI after the FFT operation will appear

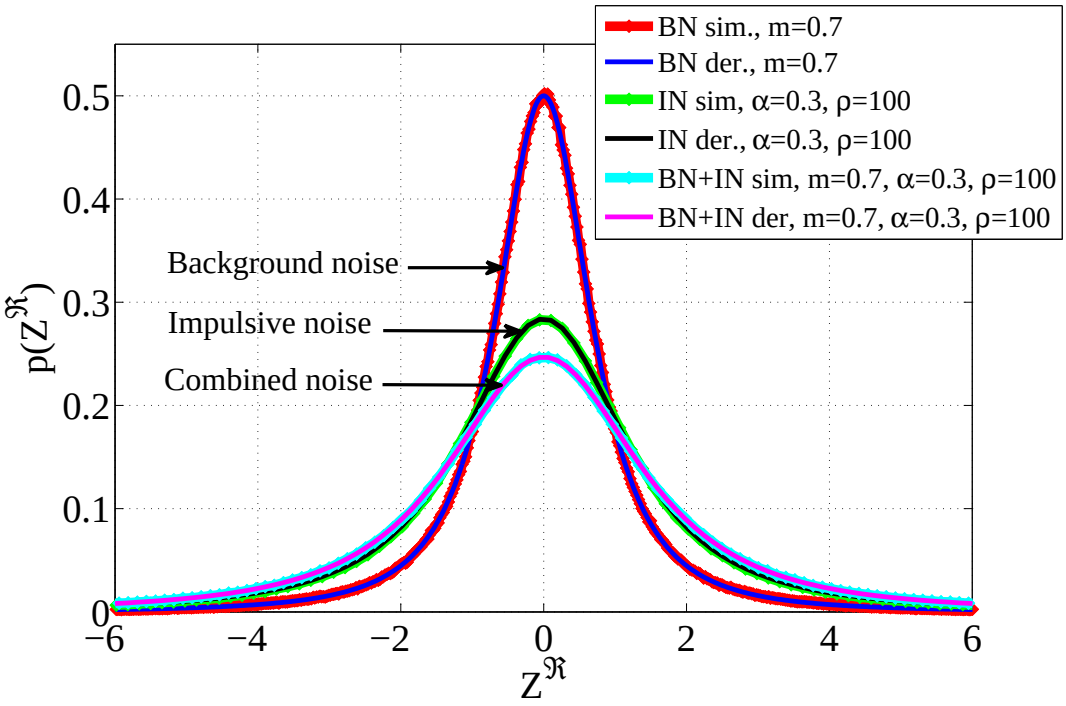

Fig. 3. Histogram plots of the equalized noise versus the derived PDFs over the PLC channel at SNR= 10 dB.

in the frequency domain as a Gaussian noise; i.e. the BER performance will depend on the average noise power as seen by the sub-carriers. Additionally, in all parameters of BI, the derived receiver outperforms the conventional receiver for all SNR values. For example, at $\mathrm{BER} = 10^{-5}$ the proposed receiver outperforms the conventional receiver and the uncoded receiver by approximately 10 dB and 30 dB, respectively.

In Fig. 4-(b), we demonstrate the BER performance of the proposed LDPC-COFDM system versus conventional LDPC-COFDM system and uncoded system. The system performances are compared in the presence of BGM only with $\alpha = 0.01, 0.1, 0.3$ and for constant $\rho = 100$, in which the obtained LLRs are computed based on the derived PDF in (28). It can be seen from the figure that the system performance degrades further in the case of BGM compared to that of BI, and as α increases the BER performance degrades for the three systems. Additionally, in all

scenarios of BGM, the derived receiver outperforms the conventional receiver that utilize blanking threshold and LLRs computed based on the Gaussian distribution due to optimal computation of the initial LLRs of SPA-LDPC decoder. For example, at $\mathrm{BER} = 10^{-5}$ the proposed receiver outperforms the conventional receiver by approximately 11, 12 and 13 dB and outperforms the uncoded receiver by approximately 33, 34 and 35 dB for $\alpha = 0.01, 0.1, 0.3$, respectively.

Fig. 5-(a) demonstrates the proposed system performance in the presence of combined Nakagami-m BI with $m = 0.7$ and BGM with $\alpha = 0.01, 0.1, 0.3$ and for constant $\rho = 100$, in which the obtained LLRs are computed based on the derived PDF in (33) versus the conventional receiver. It can be noted from the figure that the obtained BER performance degrades further compared to the BI only and BGM only cases. Moreover, the proposed receiver is very robust against combined noise even with a high impact of combined BI and BGM. In practice, the utilization of LDPC codes will reduce the requirement for the high SNR of 80 dB in the case of uncoded systems to approximately 42 dB at a BER lower than 10^{-5}, which is achievable with readily available receiver sensitivity of approximately 90 dBm. However, this requirement is further relaxed for milder multipath channels and lower levels of background interference. Furthermore, at a BER of 10^{-5}, the proposed receiver outperforms the conventional receiver by approximately 10, 12.5 and 13.5 dB and outperforms the uncoded receiver by approximately 33, 34 and 34.5 dB for $\alpha = 0.01, 0.1, 0.3$, respectively.

Fig. 5-(b) demonstrates the performance of the proposed system in the presence of combined Nakagami-m BI with $m = 0.7$ and BGM with constant $\alpha = 0.1$ and $\rho = 10, 100, 1000$ versus the conventional receiver. It can be seen from the figure that increasing ρ results in more significant BER performance degradation than increasing α. Additionally, at a BER of 10^{-5}, the proposed receiver outperforms the conventional receiver by approximately 11, 12 and 10 dB and outperforms the uncoded receiver by approximately 34, 34.5 and 33.5 dB for $\rho = 10, 100, 1000$,

respectively.

We proceed now to compare the data throughput of both systems in the presence of BI with $m = 0.7$ and BGM with $\alpha = 0.1$ and $\rho = 100$. To achieve a BER of 10^{-5} by utilizing a 4096-QAM constellation, the proposed system needs an SNR of approximately 39 dB. In contrast, for the conventional receiver to achieve the same performance an additional margin of 12.5 dB of SNR is required as shown in Fig. 5-(a) with blue lines. To compare the data throughput of both systems, the comparison needs to be performed at the same BER and SNR. Therefore, the conventional system needs to reduce the constellation size from 4096 to 512-QAM to achieve a BER level of 10^{-5} at a SNR of approximately 39 dB, as in the proposed system. This comparison is shown in Fig. 6. The resulting data throughput of the proposed and conventional systems can be then computed as 256 Mpbs and 145 Mpbs, respectively, as shown in Table II. Thus, the proposed system offers a 111 Mbps higher data throughput than the conventional system.

TABLE II

DATA THROUGHPUT COMPARISON AT BER LEVEL OF 10^{-5}

System parameters	Proposed system	Conventional system
Bandwidth (BW)	22.4 MHz	22.4 MHz
IFFT length	4096	512
Subcarriers (N)	4096	512
Subcarrier spacing(Δ_f) = $\frac{\text{BW}}{\text{IFFT length}}$	5.4688 kHz	43.75 kHz
IFFT period = $\frac{1}{\Delta_f}$	182.86 μs	22.857 μs
CP period > $\frac{d_{max}}{v_p} = \frac{1250}{1.5\times10^8}$	8.93 μs	8.93 μs
OFDM period (T) = IFFT period+CP	191.79 μs	31.787 μs
M-ary QAM	4096-QAM	512-QAM
Maximum data rate (Mbps) = $\frac{N\log_2(M)}{T}$	256 Mbps	145 Mbps

The EXIT chart analysis is shown in Fig. 7 for the noise parameters that were used to obtain

the results of Fig. 5-(a) for $\alpha = 0.1$. It can be seen from the presented trajectories that the proposed receiver requires only 7 iterations to converge compared to the 21 iterations needed by the conventional receiver. This is due to the wider opening of the EXIT chart achieved by the proposed receiver. Lower number of iterations results in reduced decoding latency, which important for the transmission of delay-sensitive, multi-media content. Furthermore, it reduces the total energy consumption of the proposed receiver.

VII. CONCLUSION

In this paper, the performance of the LDPC-COFDM system has been improved by deriving the effective noise PDF based on the ratio of complex-valued random variables at the ZF equalizer output, in which the multipath PLC channel has been taken into account. The main sources of noise in the PLC channel are the BI modelled by Nakagami-m distribution and impulsive noise modelled by the Bernoulli-Gaussian mixture model. Monte-Carlo simulations show that the performance of 4096 QAM constellation LDPC-COFDM utilizing LLRs computed based on derived PDFs outperforms the conventional receiver for different non-Gaussian noise scenarios, requiring fewer iterations to achieve convergence in EXIT chart analysis. Additionally, its offer 111 Mbps higher data throughput than the conventional system for the same SNR and BER levels.

REFERENCES

[1] Anatory, J., Theethayi, N.: 'Broadband Power-line Communications Systems: Theory & Applications', (WIT press, 2010, 1st edn.)

[2] Zimmermann, M., Dostert, K.: 'A multipath model for the powerline channel', *IEEE Trans. Commun.*, 2002, **50**, (4), pp.553-559

[3] Andreadou, N., Pavlidou, F. N.: 'Modeling the Noise on the OFDM Power-Line Communications System', *IEEE Trans. Power Deliv.*, 2010, **21**, (1), pp.150-157

[4] Zimmermann, M., Dostert, K.: 'Analysis and modeling of impulsive noise in broad-band powerline communications', *IEEE Trans. Electromagn. Compat.*,2002 , **44**, (1), pp.249–258

[5] Meng, H., Guan, Y. L., Chen,S.: 'Modeling and analysis of noise effects on broadband power-line communications', *IEEE Trans. Power Deliv.*, 2005, **20**, (2), pp. 630-637

[6] Rabie, K.M., Alsusae, E.: 'On Improving Communication Robustness in PLC Systems for More Reliable Smart Grid Applications', *IEEE Trans. Smart Grid*,2015 , **6**, (6), pp.2746-2756

[7] Kim, Y., Choi, S., Oh, H. M.: 'Closed-Form Expression of Nakagami-Like Background Noise in Power-Line Channel ', *IEEE Trans. Power Deliv.*, 2008, **23**, (3), pp.1410-1412

[8] Dario, F., and Giulio, C.: 'Theoretical limits and practical detection schemes for Markovian-Gaussian channels', *ICC'08. IEEE Inter. Conf. commun.*,2008 , pp.961–965

[9] Ghosh, M.: 'Analysis of the effect of impulse noise on multicarrier and single carrier QAM systems', *IEEE Trans. Commun.*, 1996, **44**, (2), pp.145-147

[10] Chien, Y. R.: 'Iterative Channel Estimation and Impulsive Noise Mitigation Algorithm for OFDM-Based Receivers With Application to Power-Line Communications', *IEEE Trans. Power Deliv.*,2015 , **30**, (6), pp.2435-2442

[11] Hazen, M.E.: 'The Technology Behind HomePlug AV Powerline Communications', *IEEE J. Comput.*, 2008 , **41**, (6), pp.90-92

[12] Haniph A. L., Srinivas, K., Larry, Y., et al.: 'Homeplug AV and IEEE 1901: A Handbook for PLC Designers and Users', (John Wiley & Sons, 2013, 1st edn.)

[13] John G. P.: 'Digital Communications', (McGraw-Hill, New York, 2008, 5th edn.)

[14] Zhidkov, S.V.: 'Analysis and comparison of several simple impulsive noise mitigation schemes for OFDM receivers', *IEEE Trans. Commun.*,2008 , **56**, (1), pp.5-9

[15] Juwono, F.H., Guo, Q., Chen, Y., et al.: 'Linear Combining of Nonlinear Preprocessors for OFDM-Based Power-Line Communications', *IEEE Trans. Smart Grid*, 2016 , **7**, (1), pp. 253-260

[16] Nakagawa, H., Umehara, D., Denno, S., et al.: 'A decoding for low density parity check codes over impulsive noise channels', *Proc. Inter. Symp. PLCs. and Its Appls.*, 2005, pp.85-89

[17] Tang, H., Xu, J., Kou, Y., et al.: 'On algebraic construction of Gallager and circulant low-density parity-check codes', *IEEE Trans. Inf. Theory*, 2004 , **50**, (6), pp. 1269-1279

[18] Mackay, D. J.: 'Fountain codes', *IEE Proc. Commun.*, 2005 , **152**, (6), pp. 1062–1068

[19] Mathur, A., Bhatnagar, M. R., and Panigrahi, B. K.: 'PLC Performance Analysis Over Rayleigh Fading Channel Under Nakagami- m Additive Noise', *IEEE Communs. Lett.*, 2014 , **18**, (12), pp. 2101-2104

[20] Mathur, A., Bhatnagar, M. R., and Panigrahi, B. K.: 'Performance Evaluation of PLC Under the Combined Effect of

Background and Impulsive Noises', *IEEE Communs. Lett.*, 2015 , **19**, (7), pp. 1117-1120

[21] Ten, B. S., Kramer, G., Ashikhmin, A.: 'Design of low-density parity-check codes for modulation and detection', *IEEE Trans. Commun.*,2004 , **52**, (4), pp.670-678

[22] Robert, G.: 'Low-density parity-check codes', *IRE Trans. Inf. Theory.*,1962 , **8**, (1), pp.21–28

[23] MacKay, D.J.C. and Neal, R.M.: 'Near Shannon limit performance of low density parity check codes', *E-Lett.*,1997 , **33**, (6), pp.457-458

[24] Mirahmadi, M., Al-Dweik, A., Shami, A.: 'BER Reduction of OFDM Based Broadband Communication Systems over Multipath Channels with Impulsive Noise', *IEEE Trans. Commun.*, 2013, **61**, (11), pp.4602-4615

[25] Alsusa, E., Rabie, K. M.: 'Dynamic Peak-Based Threshold Estimation Method for Mitigating Impulsive Noise in Power-Line Communication Systems ', *IEEE Trans. Power Deliv.*,2013 , **28**, (4), pp. 2201-2208

[26] Ndo, G.: 'Optimization of Impulsive Noise Countering Strategies for High Data Rate Communications over Indoor PowerLines', *Ph.D. dissertation, University of Rennes 1*, 2010

[27] Jeffrey, A., Zwillinger, D.: 'Table of Integrals, Series, and Products', (Academic Press, 2007, 7th edn.)

[28] Papoulis, A., Pillai, S. U.: 'Probability, Random Variables, and Stochastic Processes', (Tata McGraw-Hill Education, 2002, 2nd edn.)

[29] Dutka, J.: 'The Early History of the Factorial Function ', *Archive for History of Exact Sciences*,1991 , **43**, (3), pp.225-249

[30] Brink, S. T. : 'Convergence behavior of iteratively decoded parallel concatenated codes', *IEEE Trans. Commun.*,2001, **49**, (10), pp.1727-1737

[31] Bevington, P. R., Robinson, D. K., Blair, J. M., et al.: 'Data reduction and error analysis for the physical sciences', *comput phys,AIP Publishing*, 1993 , **7**, (4), pp.415–416

PLACE PHOTO HERE

Ghanim A. Al-Rubaye He received his B.Sc. and M.Sc. degrees in Electrical, Electronics and Communication from Electrical Engineering Department, College of Engineering, Al-Mustansiriya University, Baghdad, Iraq, in 1996 and 1999, respectively. He is a Lecturer in the same Department. He is currently working toward the Ph.D. degree in the School of Electrical and Electronics Engineering, Newcastle University, Newcastle Upon Tyne, U.K. His main research interests are in the area of power-line communication channels, OFDM systems, coded systems and receiver design.

Charalampos C. Tsimenidis (M'05, SM'12) is a Senior Lecturer in Signal Processing for Communications in the School of Electrical and Electronic Engineering. He received his MSc *with distinction* and PhD in Communications and Signal Processing from Newcastle University in 1999 and 2002, respectively. His main research interests are in the area of adaptive array receivers for wireless communications including demodulation algorithms and protocol design for doubly spread multipath channels. During the last 13 years has published over 180 conference and journal papers, supervised successfully 3 MPhil and 29 PhD Students and made contributions in the area of receiver design to several European funded research projects. He is a senior member of the IEEE.

Martin Johnston received the B.Sc. degree (Hons.) in physics with electronics from the Birmingham University, West Midlands, U.K., the M.Sc. degree in electronic engineering from the Staffordshire University, Staffordshire, U.K., and the Ph.D. degree from Newcastle University, Newcastle upon Tyne, U.K., in 1999, 2001, and 2006, respectively. From 2006 to 2014, he worked as a Research Associate with the School of Electrical and Electronic Engineering, Newcastle University, where he currently working as a Lecturer. His research interests include the design of advanced error-correcting schemes and low-complexity decoding algorithms for wireless communications, and data storage devices.

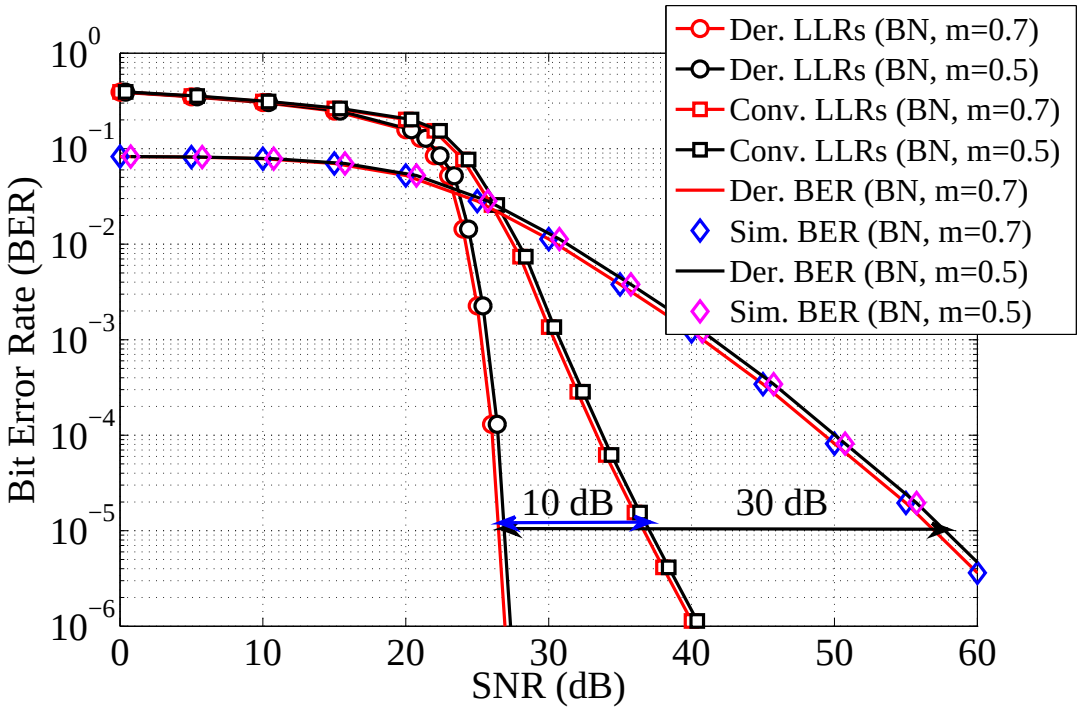

(a) BI only.

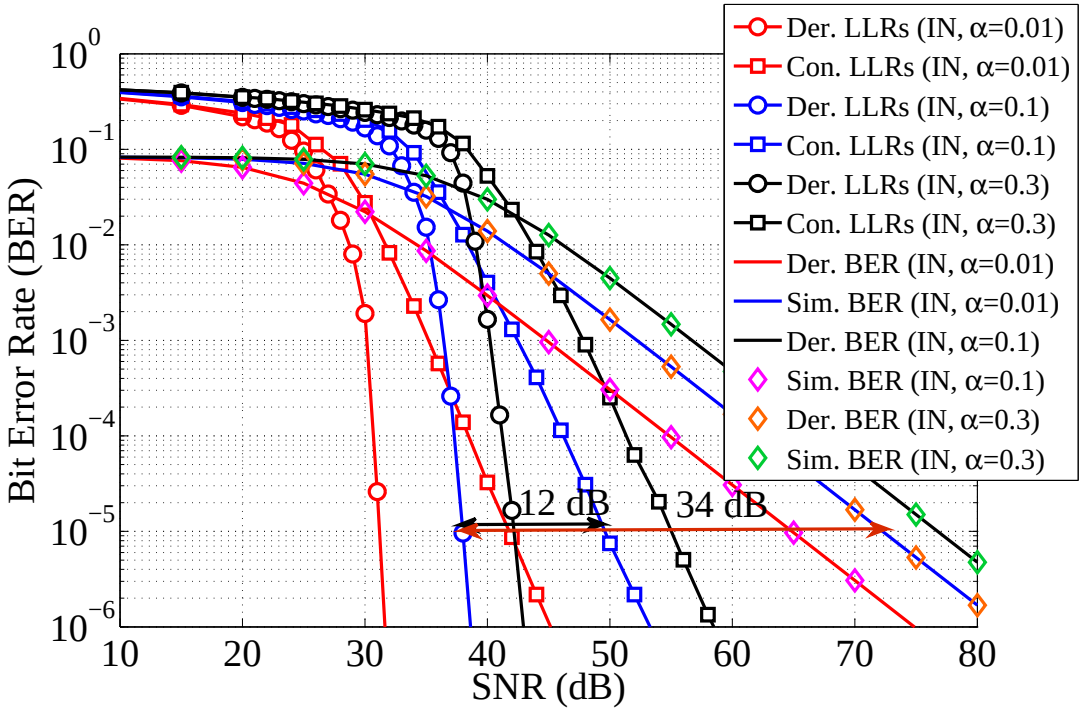

(b) IN only.

Fig. 4. Performance of the derived and conventional LDPC-COFDM versus uncoded system utilizing 4096-QAM over PLC.

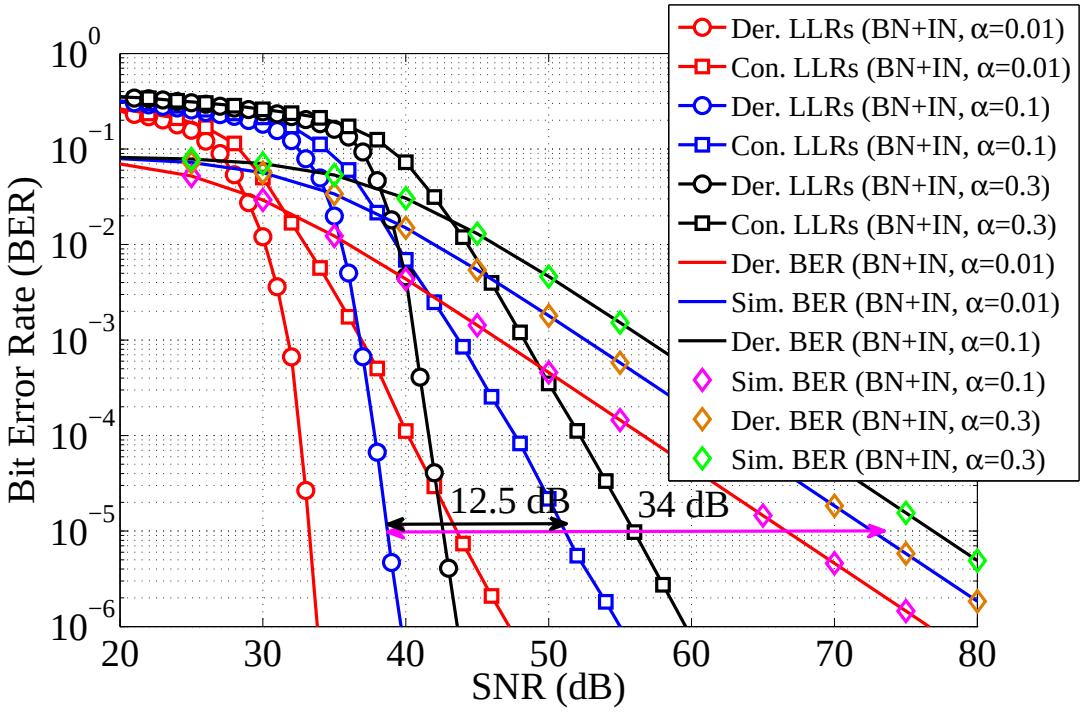

(a) α is changed.

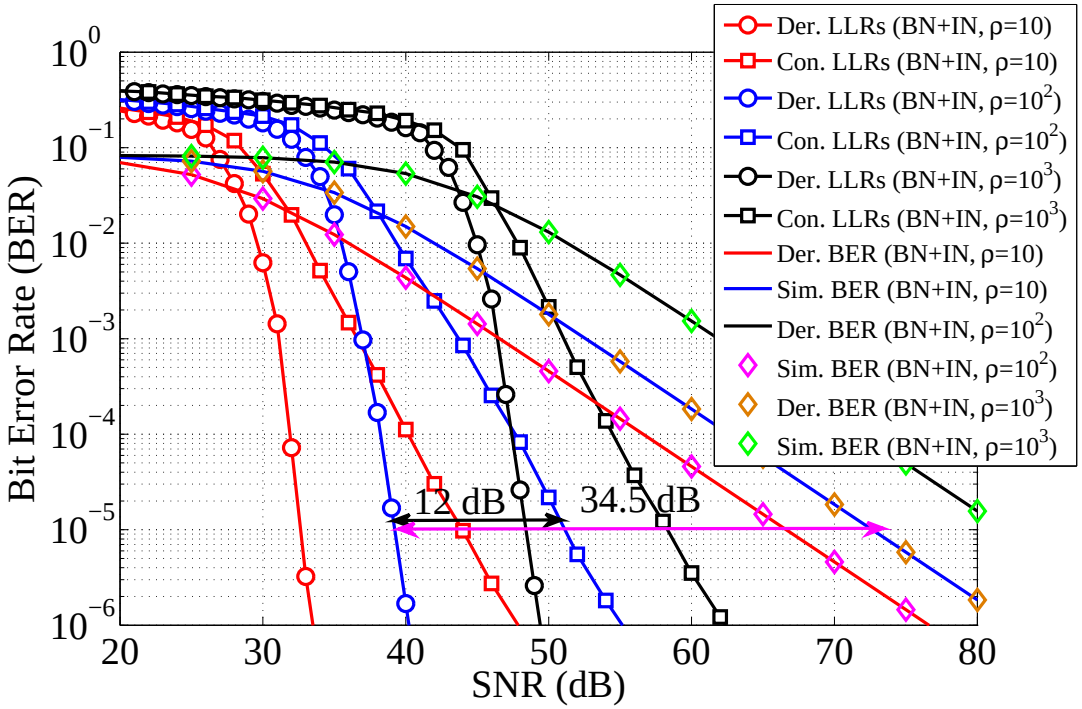

(b) ρ is changed.

Fig. 5. Performance of the derived and conventional LDPC-COFDM versus uncoded system utilizing 4096-QAM over PLC in the presence of combined BI and BGM.

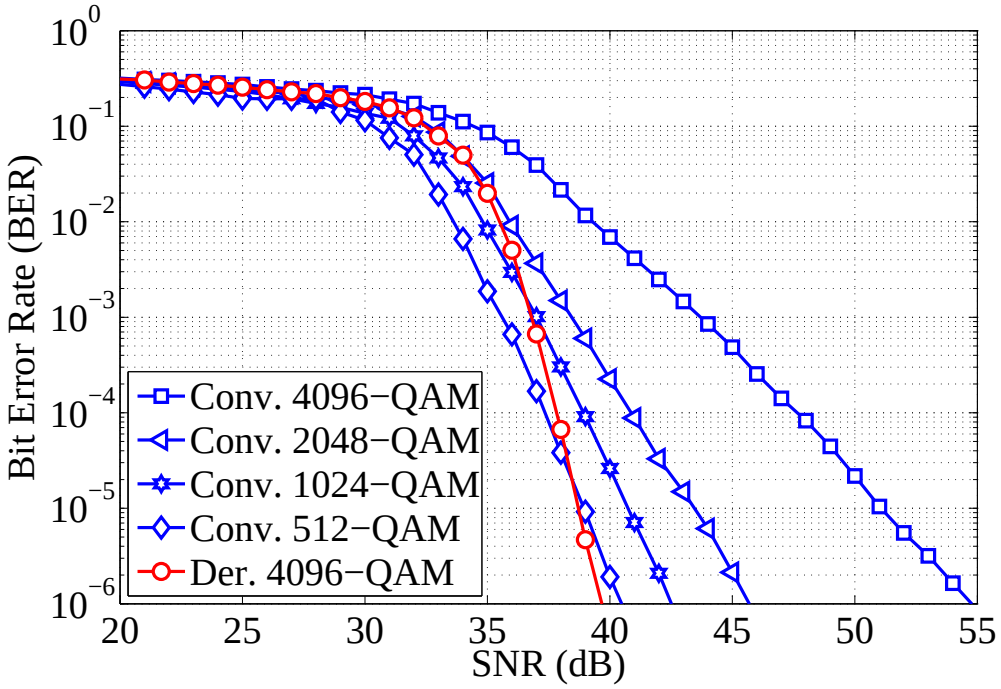

Fig. 6. Proposed LDPC-COFDM utilizing 4096-QAM versus conventional LDPC-COFDM utilizing 4096, 2048, 1024 and 512-QAM constellations over PLC in the presence of combined BI and BGM.

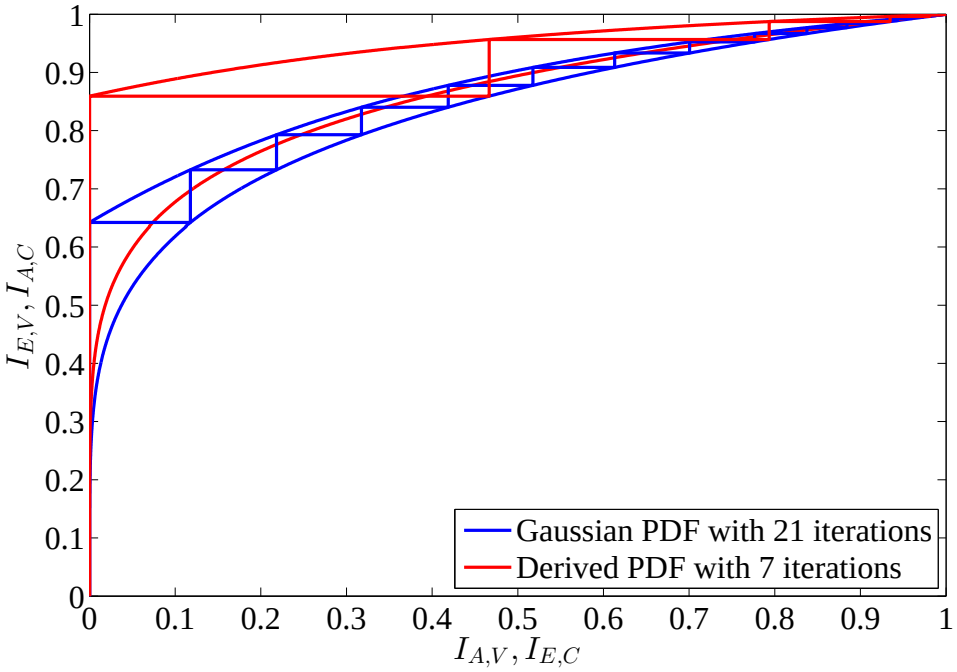

Fig. 7. EXIT Chart for LDPC-COFDM using (33) over 15-path PLC channel.